Tellus (1999), 51A, 263–272
Printed in UK – all rights reserved

TELLUS
ISSN 0280–6495

Scatterometer winds composited according to the phase of tropical intraseasonal oscillations

By ROLAND A. MADDEN*, TIMOTHY J. HOAR and RALPH F. MILLIFF, *National Center for Atmospheric Research‡, Boulder, Colorado 80307–3000, USA*

(Manuscript received 23 February 1998; in final form 22 June 1998)

ABSTRACT

Satellite measured, scatterometer winds are composited according to the longitudinal phase of upper tropospheric divergence associated with the eastward propagating, tropical intraseasonal oscillations. Results suggest that surface wind anomalies may be of global scale. They can be seen clearly in the zonal average. Accompanying anomalies in frictional torques vary by 5 Hadleys (1 Hadley $= 10^{18}$ kg m^2 s^{-2}).

1. Introduction

Scatterometer wind data provide an unprecedented opportunity to study surface winds over the world ocean. Here we try to learn more about their behavior associated with large-scale, eastward propagating, tropical intraseasonal oscillations. Measurements were made by the European Remote Sensing Satellite (ERS-1) Scatterometer. These tropical intraseasonal oscillations (hereafter designated MJO, Madden and Julian, 1994) have been shown to affect tropical circulations and clouds, and the global atmospheric angular momentum (AAM). Early, it was argued that changing frictional stresses over the tropical Pacific associated with the MJO could explain the connection to AAM (Madden, 1987; Madden, 1988; Kang and Lau, 1990). It is now known that mountain torques play an equally important role (Weickmann et al., 1992; Madden and Speth, 1995). Even though frictional stress is not the only player in the exchange of angular momentum between the atmosphere and ocean-solid earth on the MJO time-scale, it is important to fully document its effect. To date, studies of the surface winds associated with the MJO have been based on data from sparsely distributed stations over the oceans, or more frequently, on analyses from meteorological centers which are determined from the station data and characteristics of the particular analysis scheme and model. The primary focus of this study is the behavior of more comprehensively sampled ERS-1 surface winds during several MJOs, with special emphasis on changing frictional stress and torque. Our approach is to composite the wind data according to the longitudinal phase of the major convection associated with the MJO and its related upper level divergence as manifested in the 200 hPa velocity potential.

2. Scatterometer data

ERS-1 was launched in the summer of 1991. We restrict our study to the period February 1992–June 1995. The satellite scatterometer is a microwave radar (C-band) designed to measure the backscatter from the sea surface. The backscatter varies with surface geometry which, in turn, is a function of surface wind velocity. Data used

* Corresponding author.
‡ The National Center for Atmospheric Research is sponsored by the National Science Foundation.

in this study are wind vectors determined from algorithms developed at the Jet Propulsion Laboratory in Pasadena (Freilich and Dunbar, 1993). The satellite scans one 500 km wide swath per orbit. At the equator, each swath is separated by about 100 min and 2800 km (further west). Ascending (northward moving) and descending (southward moving) orbits pass over the same area at about 12-h intervals. Data are sampled within a swath at a 25-km spacing although the true resolution of the instrument is nearer 50 km. For a further discussion of the ERS-1 sampling the reader is referred to Milliff et al. (1998).

3. Compositing

The MJO is characterized by large-scale convective regions that move from the Indian Ocean to the west Pacific on a fairly regular basis. The average time between episodes is about 45 days. An episode can easily be identified in time-longitude sections of satellite cloud measurements or in the upper tropospheric velocity potential, χ. We used the latter at 200 hPa to identify the longitude of upper level divergence associated with the oscillation.* Dates were subjectively selected when the eastward propagating minima in χ, or the maximum in upper level divergence, was at 0°E, 45°E, 90°E, 135°E, 180°, 135°W, 90°W, or 45°W. Although we set no objective criteria initially, all selected episodes showed clear eastward propagation for at least 135° of longitude. We refer to these longitudinal positions as the "phase" of the MJO. During the nearly three and one-half year period, data for 128 total dates were selected. The dates were approximately evenly distributed throughout the calendar year. Table 1 lists the selected dates.

The scatterometer winds were first binned into two-degree lat/lon squares. The binned winds were then averaged over five-days centered on the dates shown in Table 1. Finally, the $2^\circ \times 2^\circ \times 5$ day averages were averaged over all dates for a given phase. Any $2^\circ \times 2^\circ \times 5$ day averages that consisted of fewer than 35 observations were considered missing. The procedure resulted in 8 wind maps, one for each selected phase of the MJO. The space-time sampling characteristics of the ERS-1 scatterometer have been studied to examine potential artifacts of bin-averaging procedures similar to the kind employed here (Chelton, 1994; Zeng and Levy, 1995). In particular, Zeng and Levy (1995) describe artifacts due to the uneven space and time distributions of samples that are then averaged to create monthly-mean fields. Artifacts of this kind probably affect the averages in our wind maps, however, our data are averaged over widely separated dates during a 3-year period and, in some cases, over nearly the entire globe. The temporal and spatial scales that characterize our signal are very large compared to the artifacts described by Zeng and Levy (1995). Therefore, we are reasonably confident that the results described below are not unduly sensitive to these artifacts.

Figure 1 shows the vector surface wind and its divergence determined from the grand average of the data regardless of the longitude of the χ minima: that is, the average of all eight maps ((3) to follow). The total number of different days averaged in Fig. 1 is slightly less than 128×5 because of occasional overlaps in the five days centered on a selected date. The wind vectors show that the averaged scatterometer data capture the trade winds and the higher latitude westerlies. Shaded areas in Fig. 1 represent regions of convergence. These regions compare well with known locations of, for example, the Intertropical and South-Pacific Convergence Zones. Although we have not compared quantitatively, the pattern over the central Pacific is similar to the 20-year average divergence presented by Stricherz et al. (1992). This gives us confidence in the representativeness of the averages of the satellite measured winds on large scales. We note that the basic wind data of Fig. 1 (and of Figs. 3 and 4 to follow) have been smoothed by a seven-point filter along latitude circles. The filter weights are 0.0417, 0.1250, 0.2083, 0.2500, 0.2083, 0.1250, 0.0417, and its half-amplitude response is about 1/8 cycle per data interval or 16° of longitude.

We wanted some measure of variability in order to assess the significance of differences between a single composite and the grand average. To that end, the variance about the 2×2 degree bin average was estimated as follows. Consider $Y_{i,j,k}$ to be the variable (zonal wind or zonal wind stress),

* Interested readers can see examples of the oscillation manifested in χ in the Climate Diagnostics Bulletin at http://nic.fb4.noaa.gov/:80/products/analysis—monitoring/bulletin/chihov.gif.

Table 1. Dates when the equatorial 200 hPa χ minimum was at the indicated longitude.

	Longitude of the 200 hPa χ minimum							
	0	45E	90E	135E	180E	225E	270E	315E
1992	02 Feb	05 Feb	09 Feb	12 Feb	16 Feb	20 Feb	—	—
1992	22 Mar	28 Mar	04 Apr*	10 Apr*	16 Apr	23 Apr	30 Apr	07 May
1992	31 May	06 Jun	13 Jun	19 Jun	25 Jun	01 Jul	07 Jul	—
1992	—	—	09 Aug	17 Aug	26 Aug	03 Sep	12 Sep	—
1992	27 Sep	04 Oct	12 Oct	19 Oct	27 Oct	—	—	—
92/93	—	—	14 Dec	18 Dec	23 Dec	28 Dec	02 Jan	—
1993	09 Jan	14 Jan	19 Jan	23 Jan	27 Jan	31 Jan	04 Feb	08 Feb
1993	28 Feb	04 Mar	07 Mar	11 Mar	14 Mar	17 Mar	20 Mar	24 Mar
1993	14 May	22 May	30 May	08 Jun	16 Jun	24 Jun	02 Jul	—
1993	—	—	22 Jul	27 Jul	01 Aug	06 Aug	12 Aug	—
1994	29 Jan	04 Feb	10 Feb	16 Feb	22 Feb	28 Feb	—	—
1994	—	—	22 Mar	29 Mar	05 Apr	12 Apr	—	—
1994	20 May	28 May	04 Jun	11 Jun	19 Jun	—	—	—
1994	—	—	27 Aug	05 Sep	14 Sep	23 Sep	03 Oct	12 Oct
1994	—	—	24 Nov	30 Nov	06 Dec	12 Dec	18 Dec	25 Dec2
94/95	—	29 Dec	08 Jan	14 Jan	20 Jan	26 Jan	31 Jan	—
1995	—	23 Feb	27 Feb	03 Mar	07 Mar	11 Mar	16 Mar	—
1995	—	—	—	—	—	—	08 Apr	17 Apr
1995	26 Apr	02 May	08 May	13 May	—	—	—	—
1995	21 May	29 May	07 Jun	16 Jun	—	—	—	—
1995	—	—	01 Jul	05 Jul	09 Jul	13 Jul	17 Jul	—
1995	—	04 Aug	08 Aug	12 Aug	16 Aug	20 Aug	24 Aug	29 Aug
1995	—	—	15 Nov	20 Nov	25 Nov	30 Nov	04 Dec	—
	11	14	21	21	20	18	16	7

Blanks are times when regular eastward propagation of χ was not evident. Two dates marked by * are those during the 1st 2 weeks of April 1992 when the satellite collected no wind data. Numbers at the bottom indicate the number of dates when the χ minimum was at a given longitude and there were scatterometer winds (K_k).

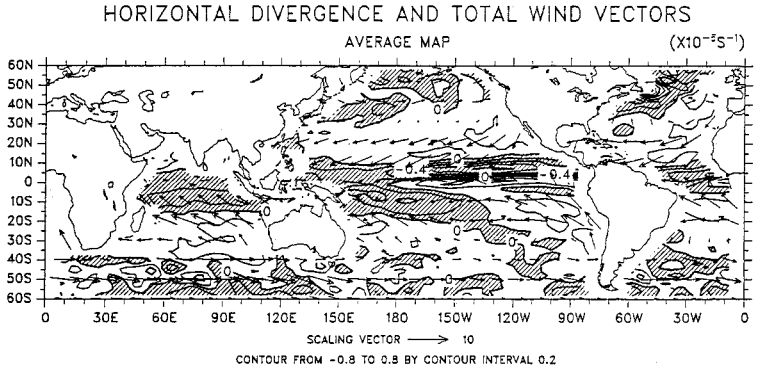

Fig. 1. The divergence of the scatterometer determined winds averaged over all dates and, as a result, all seasons (shaded regions represent convergence). Blank areas at the right and left of the figure and off shore of coasts result from a seven-point filter used to smooth these data in the east-west direction. Vectors represent a subset of determined winds. A scaling vector of a 10 m/s wind is indicated at the bottom.

where i denotes the ith observed spatial location in the 2×2 degree area on the jth day and k indicates one of the eight phases. The index j includes 5 days centered on a selected date and all the selected dates for phase k. First, the composited 2×2 degree bin average for phase k is:

$$Y_{\cdot,\cdot,k}=\frac{1}{N_k}\sum_{j}^{I_k}\sum_{i}^{I_j}Y_{i,j,k}; \tag{1}$$

I_j is the number of spatial locations available on day j, and J_k is the number of days averaged for phase k.

The sum over i for a given 2×2 degree bin averaged 15/day, and the sum over j ranged from 35 (phase 315°E) to 110 (phase 90 and 135°E).

$$N_k=\sum_{j}^{J_k}I_j, \tag{2}$$

and the grand average is:

$$Y_{\cdot,\cdot,\cdot,\cdot}=\frac{1}{8}\sum_{k=1}^{8}Y_{\cdot,\cdot,k}. \tag{3}$$

Note that each $Y_{\cdot,\cdot,k}$ is weighted equally to compute $Y_{\cdot,\cdot,\cdot,\cdot}$. A variance was also computed

$$S_k^2=\frac{1}{N_k}\sum_{j}^{J_k}\sum_{i}^{I_j}(Y_{i,j,k}-Y_{\cdot,\cdot,k})^2$$

and a pooled variance

$$S_{\cdot}^2=\frac{1}{\sum_{k=1}^{8}K_k}\sum_{k=1}^{8}K_kS_k^2,$$

where K_k is the number of dates or episodes selected for a given phase ($K_k=J_k/5$). We use an approximate t-statistic to evaluate what might be a big anomaly for a given composite;

$$T^*=\frac{(Y_{\cdot,\cdot,k}-Y_{\cdot,\cdot,\cdot,\cdot})}{[S_{\cdot}^2/K_k]^{1/2}}. \tag{4}$$

We cannot relate this quantitatively to the t-distribution because we only consider the number of episodes with a given phase (K_k) as providing additional degrees of freedom (df). The 5-day averaging and the spatial averaging over points in a 2×2 degree square introduce more df but because we do not know what the spatial and temporal dependence is, we don't know how many more df. As a result, the denominator of (4) overestimates the standard deviation of our composites. Computations are made for zonal winds and for zonal wind stresses.

4. Results

4.1. Zonal winds

We consider all selected data regardless of time of year. Fig. 2 shows composited u-wind anomalies for two extremes: when the upper level divergence is at 135°E and when it is at 90°W. The former is an average of five-days centered on each of 21 selected dates and the latter on 16 dates: totals of 110 and 80 days respectively. Stippled (hatched) regions are ones in which $T^*>1$ ($T^*<1$). Regions where $|T^*|>1$ will be referred to as "large anomalies". We can be certain that large anomalies are more than one standard deviation from the grand mean, but we don't know if they differ by more than two standard deviations given the uncertainty in the standard deviation estimate in the denominator of (4).

Fig. 2 demonstrates the transition from easterly anomalies to westerly anomalies over much of the tropical Pacific as the upper level divergence and convection move from the western to the eastern Pacific. This transition has been noted in the analyses of other data sets (Madden, 1988). There are large anomalies of the same sign as those in the tropical Pacific extending into the Atlantic. It is likely that some of these are truly part of the oscillation since surface pressure at Curacao, just off the coast of Venezuela, has been shown to be related to pressures in the Pacific in the 40–50 day period range (Madden and Julian, 1972). There are large anomalies of opposite sign over the Indian Ocean also consistent with what is known about the MJO. In addition, note some large anomalies poleward of 30° that are out of phase with those in the tropical Pacific.

We examine more closely the u-wind anomalies in the region from 30°S to 30°N. Fig. 3 is a time (phase)-longitude diagram of the 30°S–30°N zonal wind anomalies for each of the eight phases. There are no scatterometer winds available over land so the anomalies can only be averaged over ocean points. We averaged only at longitudes where observations were available at 15 or more bins out of the maximum of 30 possible between 30°S and 30°N. The familiar eastward propagation is evident. At a given phase the zero line in the surface wind anomalies falls very near the longitude of the minimum in the 200 hPa χ. The zonal average (right-hand panel, Fig. 3) shows a regular

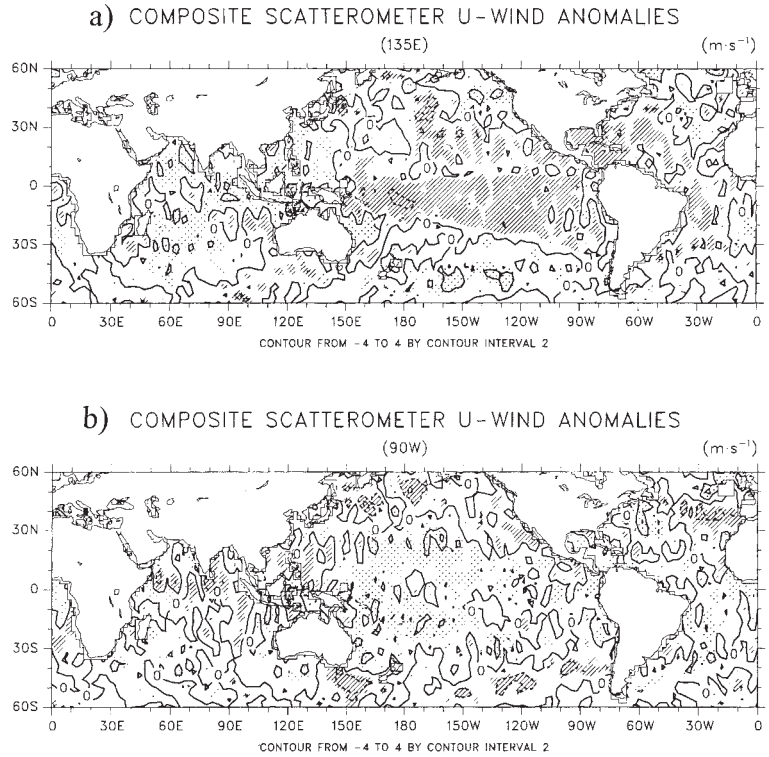

Fig. 2. Composited zonal winds for times when the 200 hPa χ minimum is at 135°E (a) and 270°E or 90°W (b). Contour interval is 2 m/s. The absolute values of most anomalies are less than 2 m/s. Stippled (hatched) regions are ones where the anomalies are "large" (see text) westerly (easterly). No spatial filtering has been applied.

cycle. This results from the fact that the amplitude variation in time of the MJO is about 1 m/s from 140°E to 150°W, while it is less than 1 m/s at other longitudes. It has been argued that the time varying zonal average is important in affecting the atmospheric angular momentum through frictional torques (Madden, 1987; Madden, 1988; Kang and Lau, 1990).

4.2. *Zonal wind stress*

Fig. 4 shows the grand average of all estimates of the zonal wind stress, τ_x, determined from

$$\tau_x = -C_D \rho u |\boldsymbol{v}| . \tag{5}$$

The density ρ was taken to be 1.2 kg m^{-3}; u is the zonal wind and $|\boldsymbol{v}|$ is the wind speed in m/s. We take the drag coefficient, C_d, from the formulation in Large et al. (1994):

$$10^3 C_D = \frac{2.70}{|\boldsymbol{v}|} + 0.142 + 0.0764|\boldsymbol{v}| \tag{6}$$

The averaging was done as in (1). The scatterometer winds capture most known features of the zonal stress field. However, the zonal average (Fig. 5), reveals that they typically give smaller absolute values for the stress than those estimated from the European Center for Medium Range Weather Forecasts (ECMWF) in the midlatitude westerlies. The ECMWF values are based on an extended (1980–1989) data set discussed by Trenberth, Large, and Olson (1989) and Trenberth, Olson, and Large (1989)*. Trenberth, Large, and Olson use a formulation of C_D that

* Data are described and available through http://www.scd.ucar.edu/dss/datasets/ds110.1.html.

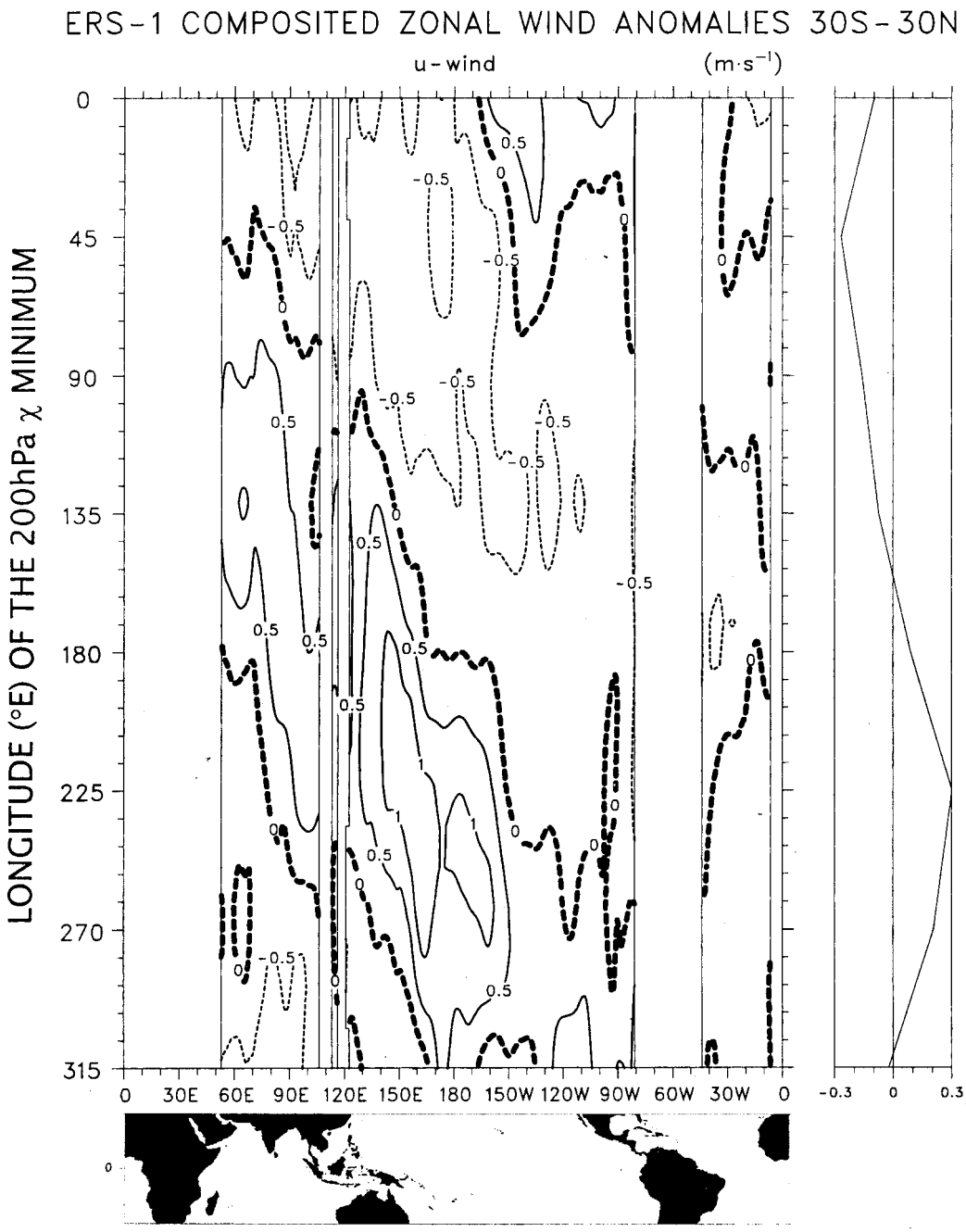

Fig. 3. Phase versus longitude diagram of the meridional average of all available composited zonal winds between 30°S and 30°N. The panel at the bottom shows the geography between 30°S and 30°N. Winds are only available over water, and values are plotted if there were 15 or more observation points at a longitude. The phase axis (ordinate) corresponds to the phase of the 200 hPa χ minimum, whose longitude (abscissa) is along a diagonal from the upper left (0, 0) to lower right (45°W, 315). The contour interval is 0.5 m/s. Right-hand panel is the zonal average. The seven-point filter was used to smooth these data in the east-west direction.

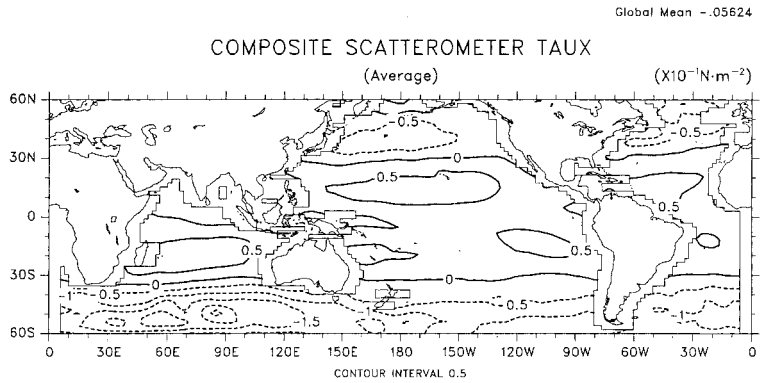

Fig. 4. Zonal wind stress (τ_x) averaged over all data. Contour intervals are 0.05 N/m^2. Dashed contours indicate regions of negative stress (westerly winds). The seven-point filter was used to smooth these data in the east-west direction.

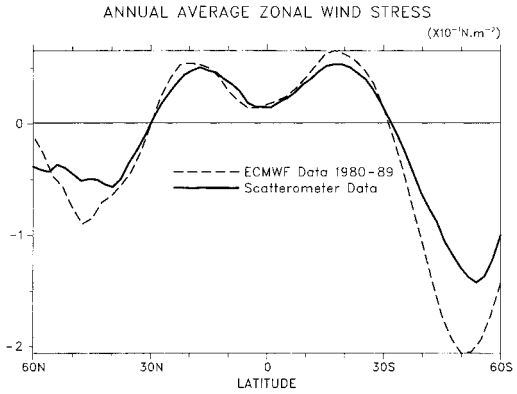

Fig. 5. The zonally averaged zonal wind stress from the scatterometer data of Fig. 4 (solid) and from 1980–1989 averaged ECMWF ocean-only winds as described in Trenberth et al. 1989 (dashed).

gives values similar to (6). They do however allow density to vary and include an effect of atmospheric boundary layer stability. The constant density of 1.2 kg/m^3 used in (5) might be closer to 1.3 kg/m^3 in colder midlatitudes. The added effects of stability contribute a few more percent but even taken together it is unlikely that these two effects can explain the differences at midlatitudes in Fig. 5. The difference at 50°S could be explained by about a 0.5 m/s difference in zonal-wind speed between the ECMWF and scatterometer winds, though the exact figure depends on total wind speed and the zonal component. It is possible that our data which only include periods of active MJO may be biased; however, Trenberth *et al.* (1989) have shown that, at least in southern latitudes, the ECMWF values exceed those of Hellerman and Rosenstein (1983) too. Our tentative conclusion is that the ECMWF stresses are too large in midlatitudes.

The composited zonal wind stress anomalies (not shown) are similar to the u-wind anomalies of Fig. 2, but not identical because of the nonlinear nature of (5). Similarly, stresses averaged from 30°S–30°N and plotted as in Fig. 3 are qualitatively the same as the similar averages of the zonal wind of Fig. 3. There is essentially a wavenumber one variation in the stress with positive values (easterly wind anomalies) to the east of the upper level divergence. The latitudinal and zonal averaged anomaly stress from 30°S–30°N, and around the world, varies regularly in the same way as the average of zonal wind (right-hand side of Fig. 3). Averaged anomaly values range from 0.0016 at phase 45°E to -0.0022 N/m^2 at phase 135°W. The stress averaged over the same area from Fig.4 is 0.0293 N/m^2. The anomaly amplitude is about one order of magnitude smaller than the average value.

An important aspect of the anomaly stresses is their changing contribution to the frictional torque. The global value of T_f, on the atmosphere is given by

$$T_f = a^3 \int_{\lambda=0}^{2\pi} \int_{\phi=-\pi/2}^{\pi/2} \tau_x \cos^2 \phi \, d\phi \, d\lambda . \qquad (7)$$

Here ϕ is the latitude, λ is the longitude, and a is the radius of the earth. Fig. 6 presents the contri-

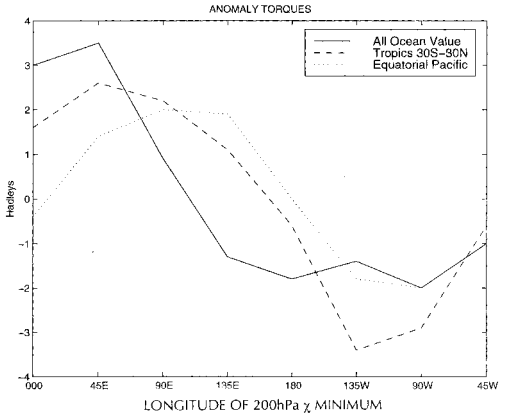

Fig. 6. Anomaly friction torque in Hadleys (1 Hadley = 10^{18} kg m^2 s^{-2}) for each of the eight phases. Phases or longitude of the 200 hPa χ minima are indicated along the abscissa.

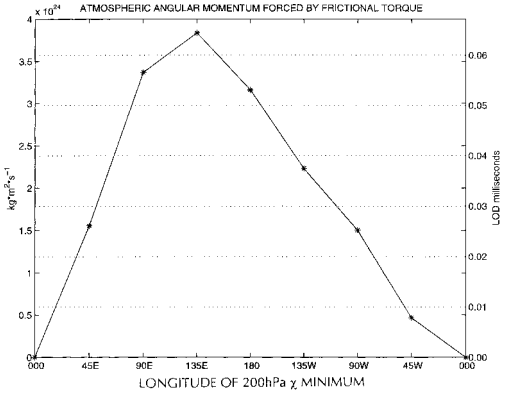

Fig. 7. The integral of the all-ocean frictional torque of Fig. 6 showing anomalies in atmospheric angular momentum that would result. Assumptions are that the anomaly torque evaluated at each phase acts for 6-days and that angular momentum anomaly is zero at the start of the integration. The right-hand scale is a change in the length-of-day that corresponds to the angular momentum anomaly.

bution to the friction torque from all ocean areas 60°S to 60°N. Largest negative anomalies occur when the upper level divergence is between 135°E through 45°W. A substantial part of the all-ocean value can be explained by that contributed by the 30°S–30°N band which is also shown in Fig. 6 (dashed line). Madden (1988) studied frictional stresses over the tropical Pacific, and argued that associated changes in global, frictional torque could be accounted for by contributions from that limited area. For comparison, we have included the contribution to the torque from the equatorial Pacific region bounded by 30°S, 30°N, 140°E, and 90°W … . We see that the reduced region contributes about two thirds of the all-ocean value but the time of its maximum is shifted one phase later.

Fig. 7 shows the time variation of total AAM that would result from the all-ocean frictional torques of Fig. 6. To arrive at Fig. 7, the values of Fig. 6 were multiplied by the number of seconds in a day and by six days (86400×6), assuming a 48-day period for the 8 phases. It was arbitrarily assumed that at phase 0°E the anomaly in the angular momentum was zero. To put the resulting changes of 4×10^{24} kg m^2 s^{-1} shown Fig. 7 in perspective, we recall that the seasonal variation in M is between 50 and 75×10^{24} kg m^2 s^{-1} (Rosen and Salstein, 1983). The anomaly during the El Niño of January 1983 found by Rosen et al. (1984) was near 14×10^{24} kg m^2 s^{-1} (assuming an approximate average January value of 180×10^{24} kg m^2 s^{-1} and the 8% increase they reported).

Fig. 7 also has a length-of-day (LOD) scale. An anomaly in M is related to one in LOD by

$$\Delta\mathrm{LOD} = 1.68 \times 10^{-26} \Delta M, \qquad (8)$$

where ΔM is kg m^{2}s$^{-1} \times 10^{26}$ and ΔLOD is in milliseconds (Rosen and Salstein, 1983).

We see that the average change in *LOD* forced by the intraseasonal oscillations is just less than 0.07 ms. It can be nearly an order of magnitude greater for individual oscillations (Madden, 1988).

5. Discussion

The scatterometer winds provide an excellent set of observations for monitoring surface winds over the oceans. Here we have used them to study changing winds associated with the evolving MJO. The results confirm and further quantify other studies based on less spatially comprehensive data. There are very large-scale variations in the surface winds, primarily over the central Pacific. When averaged from 30°S–30°N their amplitude is about 1 m/s near the Date Line. Even zonal averages of these 30°S–30°N winds vary from nearly −0.3 m/s when the convective activity is in the Indian Ocean

to +0.3 m/s when it has dissipated and the upper level minimum in χ is near 135°W. Indeed, the anomalies of the equatorial Pacific may extend into the Caribbean and Atlantic Oceans. There also appear to be large opposite phase (from the equatorial Pacific) anomalies in the Indian Ocean and in the westerlies poleward of 30°.

Anomalies in zonal wind stress are qualitatively similar to those of the zonal winds. Resulting changes in frictional torque range from +3 Hadleys to −2 Hadleys when considering all available ocean points from 60°S–60°N. Maxima occur when convective activity is building in the Indian Ocean and minima occur when it has weakened near and east of the Date Line. The region of the equatorial Pacific from 30°S–30°N and from 140°E–90°W contributes about two thirds of these frictional torque anomalies. Values from that limited region reach their maximum after the all-ocean values at about the time the minimum in the 200 hPa χ field leaves the Indian Ocean and enters the western Pacific. The change in atmospheric angular momentum due to changes of this size in torque over a 48-day period would be 4×10^{24}, or roughly one order of magnitude smaller than those associated with the seasonal change.

Undoubtedly anomalies are dependent on season. Results presented here are averaged over all seasons. We did stratify our results into April–September and October–March periods but we detected no certain changes from that described above. Further investigation of seasonal changes will have to await the collection of more scatterometer data.

6. Acknowledgements

E. C. Rothney prepared the manuscript. Timothy J. Hoar is supported by the Geophysical Statistics Project at NCAR under NSF Grant No. DMS-9312686. Ralph F. Milliff is supported through a NASA Interagency Agreement for the NSCAT Science Working Team at NCAR.

REFERENCES

Chelton, D. B. 1994. *The space-time resolution capability of surface wind fields constructed from ERS-1 scatterometer data*. NASA Scatterometer Science Working Team Meeting Report, 1–3 June 1994, Kona, HI, 102–113.

Freilich, M-H. and R. S. Dunbar, 1993. A preliminary C-Band scatterometer model function for the ERS-1 AMI instrument. *Proceedings 1st ERS Symposium-Space at the service of our environment*. Cannes, 4–6 November 1992.

Hellerman, W. and M. Rosenstein, 1983. Normal monthly wind stress over the world ocean with error estimates. *J. Phys. Oceanogr.* **13**, 1093–1104.

Kang, I.-S. and K.-M. Lau, 1990. Evolution of tropical circulation anomalies associated with 30–60 day oscillation of globally averaged angular momentum during northern winter. *J. Meteor. Soc. Japan* **68**, 237–249.

Large, W. G., J. C. McWilliams, and S. C. Doney, 1994. Oceanic vertical mixing: A review and a model with a nonlocal boundary layer parameterization. *Rev. of Geophys.* **32**, 363–403.

Madden, R. A. 1987.Relationships between changes in the length of day and the 40 to 50 day oscillation in the tropics. *J. Geophys. Res.* **92**, 8391–8399.

Madden, R. A. 1988. Large intraseasonal variations in wind stress over the tropical Pacific. *J. Geophys. Res.* **93**, 5333–5340.

Madden, R. A. and P. R. Julian, 1972. Description of global-scale circulation cells in the tropics with a 40–50 day period. *J. Atmos. Sci.* **29**, 1109–1123.

Madden, R. A. and P. R. Julian, 1994. Observations of the 40–50 day tropical oscillation. A review. *Mon. Wea. Rev.* **122**, 814–837.

Madden, R. A. and P. Speth, 1995. Estimates of atmospheric angular momentum, friction, and mountain torques during 1987–1988. *J. Atmos. Sci.* **52**, 3681–3694.

Milliff, R. F., T. J. Hoar, and R. A. Madden, 1998. Fast, eastward moving disturbances in the surface winds of the Equatorial Pacific. *Tellus* **50A**, 26–41.

Rosen, R. D. and D. A. Salstein, 1983. Variations in atmospheric angular-momentum on global and regional scales and the length of day. *J. Geophys. Res.* **88**, 5451–5470.

Rosen, R. D., D. A. Salstein, T. M. Eubanks, J. O. Dickey, J. A. Steppe, 1984. An El Niño signal in atmospheric angular momentum and earth rotation. *Science* **225**, 411–414.

Stricherz, J. N., J. J. O'Brien, and D. M. Legler, 1992. *Atlas of Florida State University Tropical Pacific Winds for TOGA 1966–1985*. Mesoscale Air-Sea Interaction Group Technical Report, The Florida State University, Tallahassee, FL 21 pp.

Trenberth, K. E., W. G. Large, and J. G. Olson, 1989. The effective drag coefficient for evaluating wind stress over the oceans. *J. Climate* **2**, 1507–1516.

Trenberth, K. E., J. G. Olson, and W. G. Large, 1989. A global ocean wind stress climatology based on ECMWF analyses. NCAR/TN-338+STR, 93 pp.

Weickmann, K. M., S. J. S. Khalsa, and J. Eischeid, 1992. The angular momentum cycle during the tropical Madden-Julian oscillation. *Mon. Wea. Rev.* **120**, 2252–2263.

Zeng, L. and G. Levy, 1995. Space and time aliasing structure in monthly mean polar-orbiting satellite data. *J. Geophys. Res.* **100**, 5133–5142.